Geophysical Research Letters

An Externally Forced Decadal Rainfall Seesaw Pattern Over the Sahel and Southeast Amazon

Wenjian Hua[1,2] (iD), Aiguo Dai[2] (iD), Liming Zhou[2] (iD), Minhua Qin[1,2] (iD), and Haishan Chen[1] (iD)

[1]Key Laboratory of Meteorological Disaster, Ministry of Education (KLME)/Joint International Research Laboratory of Climate and Environment Change (ILCEC)/Collaborative Innovation Center on Forecast and Evaluation of Meteorological Disasters (CIC-FEMD), Nanjing University of Information Science and Technology, Nanjing, China, [2]Department of Atmospheric and Environmental Sciences, University at Albany, State University of New York, Albany, NY, USA

Abstract By analyzing observations and model simulations, here we show that there exists a significant anticorrelation on interannual to multidecadal time scales between the Sahel and southeast Amazon rainfall during July-August-September. This rainfall seesaw, which is strongest on decadal to multidecadal scales, is due to an anomalous meridional gradient of sea surface temperatures across the tropical Atlantic that pushes the Intertropical Convergence Zone and its associated rain belt toward the anomalously warm hemisphere. Large ensemble model simulations suggest that the seesaw pattern is likely caused by decadal changes in anthropogenic and volcanic aerosols, rather than internal climate variability. Our results suggest that the recent decadal to multidecadal climate variations in and around the North Atlantic basin are largely externally forced and that projected large North Atlantic warming could lead to a wetter Sahel but drier Amazon in the future.

Plain Language Summary Both the semiarid Sahel and Amazon rain forest are known hot spot regions of climate change. However, the causes of Sahelian and Amazonian rainfall variations are still debated and the scientific community has often examined these two regions separately rather than collectively. Here we show that there exists a significant decadal rainfall seesaw pattern between the Sahel and southeast Amazon during July-August-September in observations and coupled model simulations. This seesaw pattern is likely caused externally by decadal changes in anthropogenic and volcanic aerosols, rather than internal climate variability. Our findings not only detect and attribute the seesaw pattern over the Sahel and Amazon Basin but also provide further evidence for major impacts of external forcing on recent decadal climate variations in and around the North Atlantic Ocean.

1. Introduction

The semiarid Sahel region of West Africa suffered from a severe drought during the 1970s and 1980s and has exhibited an upswing of rainfall since the 1990s (Dai et al., 2004; Folland et al., 1986; Giannini et al., 2003). The unprecedented Sahelian drought has been attributed to the larger warming in the southern than in the northern tropical Atlantic (Hoerling et al., 2006; Lamb & Peppler, 1992), Indian Ocean warming (Hagos & Cook, 2008; Palmer, 1986), and anthropogenic forcings (Biasutti & Giannini, 2006; Held et al., 2005). Compared with the extensive research on the Sahelian decadal drought, relatively few studies have examined the recent rainfall recovery, with increasing greenhouse gas (GHG) forcing (Dong & Sutton, 2015) and the Mediterranean Sea warming (Park et al., 2016; Rowell, 2003) being considered as the main drivers. It remains unclear whether external factors (e.g., GHGs and aerosols) or internal sea surface temperature (SST) variability dominates the Sahelian rainfall variability (e.g., Monerie et al., 2017).

The rainy season in the Sahel corresponds to the Amazonian dry season from July to September (Figure S1 in the supporting information). With massive impacts on world's biodiversity and climate, the Amazon has recently experienced severe droughts in 2005, 2010, and 2016, which have attracted worldwide attention (Cox et al., 2008; Lewis et al., 2011; Marengo et al., 2011; Zeng et al., 2008), as changes in rainfall patterns, particularly in the dry season, will determine the future fate of the Amazon rainforest (Malhi et al., 2008). Rainfall in the Amazon is most sensitive to the interannual to decadal SST variations in the tropical Pacific and Atlantic Oceans, but the influences of SSTs vary by season and region (Yoon & Zeng, 2010; Zeng et al., 2008). For example, Atlantic SSTs are typically linked to the dry-season rainfall in western Amazonia (Cox et al., 2008) and the streamflow in Amazon Rivers (Marengo et al., 2011).

Both the Sahel and Amazon Basin are known hot spot regions of climate change. Understanding their rainfall variability therefore has significant scientific, economical, and societal implications. However, previous studies have often examined these two regions separately rather than collectively. Baines and Folland (2007) showed that the changes in the tropical regions (e.g., the Sahel, the Caribbean, and the Brazil) are approximately coincident through an empirical orthogonal function analysis and may be partly linked to the climate shift of the late 1960. Furthermore, significant correlations between Atlantic SST and Sahelian or Amazonian rainfall variations have been found separately (e.g., Cox et al., 2008; Fernandes et al., 2015; Martin et al., 2014; Shanahan et al., 2009; Zhang & Delworth, 2006). This would imply a relationship of rainfall between the two regions. However, the exact cause of this rainfall link between the Sahel and southeast Amazon (SA) is not well understood. In particular, the role of internal variability (IV) and external forcing in generating the recent rainfall variations over these regions remains unclear. Here we present evidence for a robust rainfall seesaw pattern between the Sahel (10°N to 20°N, 10°W to 30°E) and SA (18°S to 0°N, 45°W to 65°W) on interannual to multidecadal time scales during the July-August-September (JAS) season and explore its underlying mechanisms by analyzing observational data and model simulations. Our findings should help uncover the nature and cause of the JAS rainfall variability in the wet-season Sahel and the dry-season Amazon and improve predictions of future droughts over both regions. Our results also contribute to the current debate about the origin of the Atlantic Multidecadal Oscillation (AMO; Vecchi et al., 2017) and provide further evidence for a major role of external forcing in recent AMO.

2. Data, Model Simulations, and Methods

2.1. Observational and Reanalysis Data

The primary long-term monthly rainfall data set used in this study is the Global Precipitation Climatology Centre Full Data Product V7 on a 1° grid from 1901 to 2013 (Schneider et al., 2014). Rainfall data from 2014 to 2017 were based on the Global Precipitation Climatology Centre's V4 monitoring product. To ensure the robustness of our results, we also examined four other global precipitation data sets, including the Climatic Research Unit TS v4.01 (Harris et al., 2014), the Global Historical Climatology Network (Jones & Moberg, 2003; Peterson & Vose, 1997), the National Oceanographic and Atmospheric Administration (NOAA) PRECipitation REConstruction over Land (Chen et al., 2002), and the precipitation product from the University of Delaware (Willmott & Matsuura, 2001). These five data sets differ in spatial resolution, observational data sources, data quality controls, and analysis methods (Table S1); however, they show similar and consistent rainfall variations over the Sahel and SA during JAS (Figure S2).

We used the merged Hadley-OI SST data set created by Hurrell et al. (2008), who merged the Hadley Centre's SST data set, which was derived by gridding bias-adjusted in situ observations, with the NOAA weekly optimal interpolation (OI) analysis. The Hadley Centre's SST data set spanned 1870 onward, whereas the OI started in November 1981. This product takes advantage of the higher-resolution SST of the NOAA OI data set. Monthly data for 850-hPa geopotential height and winds were obtained from the National Centers for Environmental Prediction/National Center for Atmospheric Research reanalysis (Kalnay et al., 1996).

2.2. Climate Model Simulations

We analyzed the large ensembles of fully coupled climate model simulations using the Canadian Earth System Model version 2 (CanESM2; Kirchmeier-Young et al., 2017). These 50-member ensemble simulations at T42 grid spacing (~2.8°) were started with slightly different initial conditions and forced by all historical forcings (ALL) from 1950 to 2005 and with Representative Concentration Pathway (RCP8.5) forcing thereafter. Besides this ALL forcing ensemble, we also used two other 50-member ensembles of CanESM2 simulations with natural forcing (NAT) only and with anthropogenic aerosols (AA) forcing only.

We also used coupled climate model simulations from the phase 5 of the Coupled Model Intercomparison Project (CMIP5; Taylor et al., 2012). The effects of different historical external forcing agents were investigated by analyzing simulations forced by ALL, NAT, AA, and RCP4.5 forcing (Table S2). We chose those CMIP5 models that provided more ensemble realizations or had the ALL, NAT, and AA experiments for our analysis. All the model data were regridded onto a common 2.5° × 2.5° grid using bilinear spatial interpolation.

Stratospheric aerosol optical thickness was used to quantify volcanic forcing in the CMIP5 simulations (Sato et al., 1993). We used the estimated stratospheric aerosol optical depths at $\lambda = 550$ nm (https://data.giss.nasa.gov/modelforce/strataer/) to represent the volcanic activities. We used total solar irradiance data (http://solarisheppa.geomar.de/cmip6) to represent the variations in solar irradiance (Lean, 2000; Wang et al., 2005). To represent the GHG forcing, we simply used the observed atmospheric CO_2 concentration since 1958 at Mauna Loa Observatory, Hawaii (https://www.esrl.noaa.gov/gmd/ccgg/trends/data.html).

2.3. Methods

We analyzed multiple rainfall data sets over the Sahel (10°N to 20°N, 10°W to 30°E) and SA (18°S to 0°N, 45°W to 65°W) and focused on the 3-month period of JAS. To examine the rainfall variations and the changes in atmospheric circulation, we performed regression analyses between the atmospheric circulation anomaly fields and regional rainfall time series. A linear correlation coefficient (r) and its significance level (p value) were calculated between two time series to quantify their association. To remove short-term variability, 11-year running averaging was applied to most time series before correlation and regression analyses. Statistical significance tests were based on the Student's t test with reduced degree of freedom accounting for autocorrelations (Zhao & Khalil, 1993).

We characterized the AMO or Atlantic Multidecadal Variability via an index based on the area-averaged North Atlantic SST (0–80°W and 0–60°N) anomalies by removing the SST anomalies averaged over the global oceans (60°N to 60°S) following Trenberth and Shea (2006). The SST anomalies were further smoothed using 11-year running means. To quantify the variations in tropical Atlantic SST meridional gradient associated with Sahel and SA rainfall variations, an Atlantic north-south SST gradient (ANSG) index was defined as the SST difference between the low-latitude North Atlantic (15–75°W and 5–30°N) and the low-latitude South Atlantic (40°W to 20°E and 5°S to 30°S).

The ensemble mean of climate simulations from a single climate model can provide a good estimate of the forced signal, as the uncorrelated internal variations among the individual simulations are greatly reduced during this averaging (Dai & Bloecker, 2018; Frankcombe et al., 2018). The CanESM2 performs well in simulating the regional rainfall, North Atlantic SSTs, and North Atlantic subsurface ocean heat content and salinity (supporting information S1). We therefore used the arithmetic mean of the 50 members from the CanESM2 ensemble runs as the first-order estimate of the forced signal and removed it from observations or individual model runs to produce the residual fields that contain primarily IV (Dai et al., 2015; Frankcombe et al., 2015; Hua et al., 2018; Steinman et al., 2015; see supporting information and section 2.3 for more information). We also used CMIP5 multimodel ensemble mean as an estimate of the forced signal.

3. Results

3.1. Observed Rainfall Seesaw Pattern

Sahel rainfall data show drier conditions for JAS before the mid-1920s and relatively wet conditions from the mid-1920s to 1960s, whereas the SA rainfall generally experienced the opposite variations despite data paucity during the early twentieth century (not shown). Here we focus on the period from 1950 onward when rainfall data are more reliable for both regions. The JAS rainfall anomalies during 1950–2017 over the two regions are negatively correlated ($r = -0.43$, $p < 0.01$; Figure 1a). This anticorrelation becomes stronger ($r = -0.87$, $p < 0.01$) on decadal to multidecadal scales, with negative (positive) anomalies from the late 1960s to mid-1990s and positive (negative) anomalies in the 1950s and early 1960s and after the late 1990s in the Sahel (SA; Figure 1a). Such covariability is robust across the five widely used precipitation data sets, which all show strong and similar decadal to multidecadal variations (Figure S2), with the decadal anticorrelation ranging from −0.79 to −0.89 ($p < 0.01$). Thus, there exists a robust JAS rainfall seesaw pattern linking the Sahel and the SA, especially on decadal to multidecadal time scales. We also examined other seasons and found that such an anticorrelation becomes insignificant, for example, during Amazon's wet season (January–March).

To investigate the cause of this seesaw pattern in JAS, we first examine the regression patterns of SST, 850-hPa geopotential height, and winds against the regional rainfall anomaly over both regions. A warm anomaly in the North Atlantic and a weak cold anomaly in the South Atlantic are associated with positive
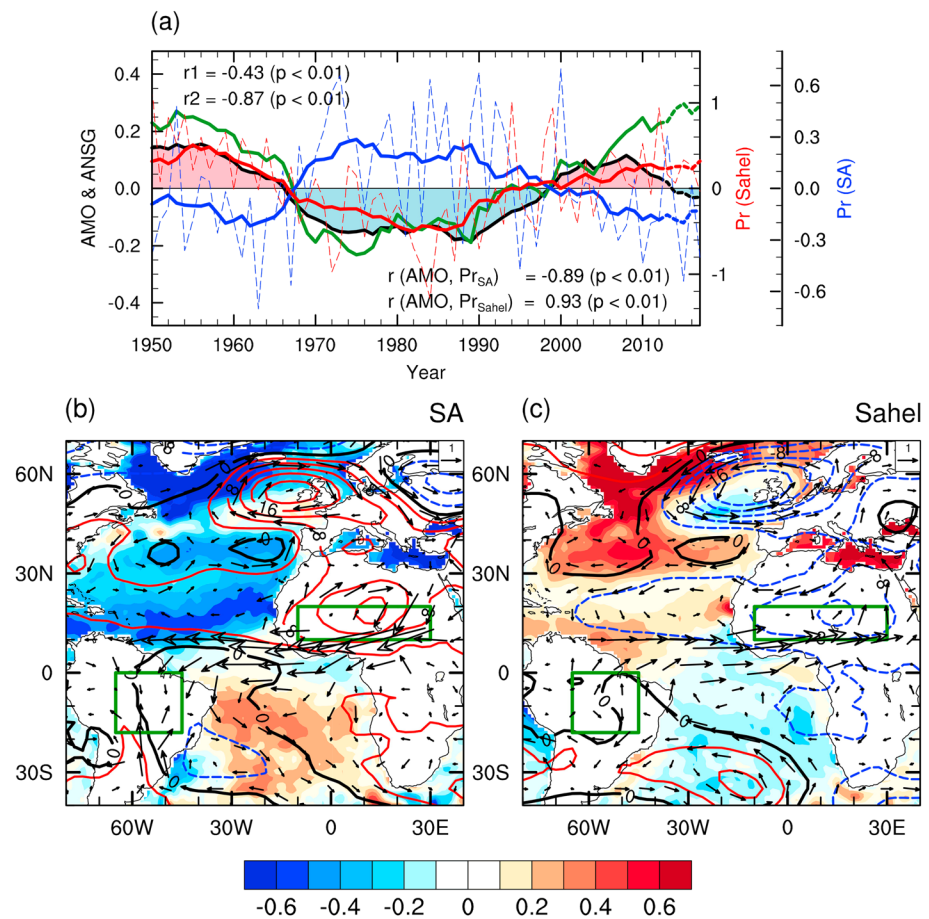
Figure 1. (a) Time series of observed July-August-September detrended rainfall anomalies (dashed lines, mm/day) with an 11-year running average (solid lines) superimposed for the Sahel (in red) and Southeast Amazon (SA, in blue). Also shown are the 11-year smoothed Atlantic Multidecadal Oscillation (AMO; black line with shading) and the Atlantic North-South SST gradient (ANSG) index (green line). The $r1$ ($r2$) is the correlation coefficient between the dashed (solid) red and blue lines, together with the attained significance level (p). The correlation coefficients r between the smoothed AMO index and the two regional rainfall series are also shown. The last 5 years, plotted using dashed, used mirrored data in the running average and thus is less reliable. Regression patterns of the SST (shading, °C), 850-hPa geopotential height (contours, gpm) and wind (vectors, m/s) fields onto the July-August-September detrended rainfall anomalies over (b) SA and (c) the Sahel. The rectangular boxes in (b) and (c) indicate the Sahel and SA regions.

(negative) Sahel (SA) rainfall anomalies (Figures 1b and 1c), indicating that a change in the ANSG is key for the rainfall seesaw pattern. Previous studies have shown that Sahel rainfall variations are strongly related to SST anomaly patterns in the tropical Atlantic (e.g., Baines & Folland, 2007; Folland et al., 1986; Sheen et al., 2017). The Atlantic influence is manifested through changes in the atmospheric circulation and the movement of the intertropical convergence zone (ITCZ) that follows the warmest SST zone in the Atlantic (Figures 1b and 1c). This meridional movement of Atlantic ITCZ is remarkable during Amazon's dry season, which corresponds to Sahel's rainy season in JAS (Figure S1). The SA becomes wetter when the North Atlantic is relatively cold than the South Atlantic, which leads to northerly winds over north of the equator and a southward shift of the ITCZ. This southward shift increases (decreases) rainfall over SA (the Sahel) due to the sharp meridional rainfall gradients around the two regions (Figure S1). Warm SST anomalies and anomaly cyclonic circulations are seen in the South Atlantic during SA wet periods (Figure 1b). This enhances the southerly winds and moisture convergence into the SA and increases rainfall there. Similarly, the Sahel becomes wetter when the North Atlantic is warmer than the South Atlantic, which leads to a low-pressure anomaly over West Africa and surrounding areas (Figures 1b and 1c). This enhances southwesterly winds into the Sahel and causes a northward shift of the ITCZ and increase rainfall in the Sahel. These changes all suggest that the rainfall seesaw pattern is

AGU
100
ADVANCING EARTH
AND SPACE SCIENCE

Geophysical Research Letters

10.1029/2018GL081406
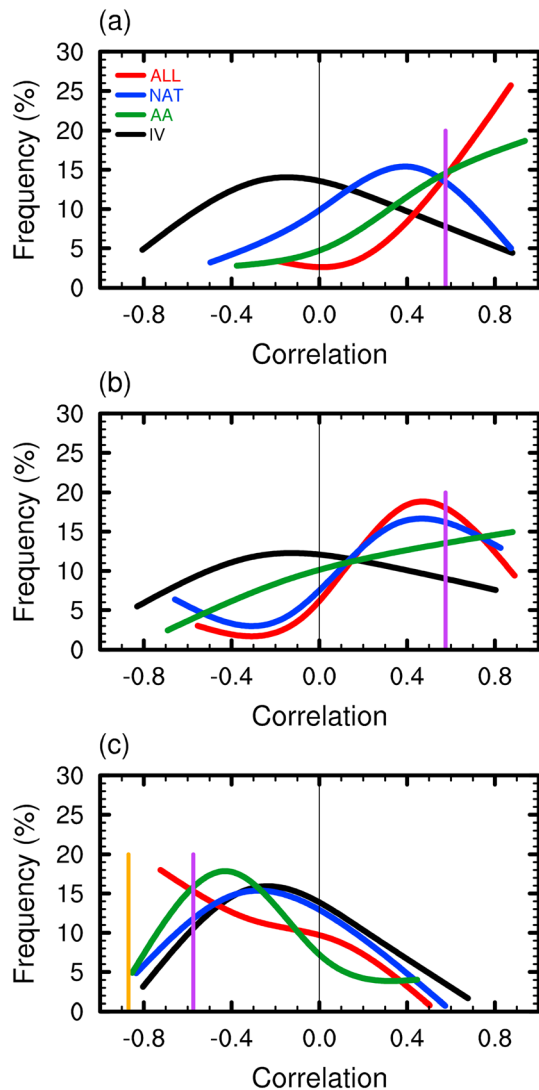
Figure 2. (a) Estimated histograms of the correlation coefficients during 1950–2017 between the 11-year smoothed observed and CanEMS2-simulated Sahel July-August-September rainfall (after linear detrending and 11-year running averaging) from individual model runs with all-forcing (ALL, red line), natural forcing only (NAT, blue line), and anthropogenic aerosol forcing only (AA, green line). The black line is for the internal variability (IV) case, in which the Sahel July-August-September rainfall series from 150 individual members from the ALL, NAT, and AA simulations were first subtracted by their respective ensemble mean, smoothed with 11-year averaging, and then correlated with the 11-year smoothed rainfall series from observations. A cubic spline was fitted to the histograms to produce the smooth curves shown here. (b) Same as (a) but for southeast Amazon. (c) Estimated histograms of decadal rainfall correlations between the Sahel and southeast Amazon from the Canadian Earth System Model version 2 ALL, NAT, AA, and IV simulations during 1950–2017. The purple vertical lines in (a to c) indicate the r values above it (or below it in c) are statistically significant at the 0.05 level for all the four cases. The orange line in (c) represents the observed correlation coefficient during the same period.

associated with the large-scale interhemispheric variations in Atlantic SSTs and related atmospheric circulation changes across the Sahel and SA.

Figure 1a shows that Sahel and SA decadal rainfall variations are highly correlated with the ANSG, as well as the AMO. The basin-wide SST anomalies over the North Atlantic Ocean shown in Figures 1b and 1c resemble the AMO pattern, and the decadal rainfall variations over the Sahel and SA correspond well to the AMO phase changes (Figures 1a and S2). Previous studies have shown significant correlations between Atlantic SST and Sahelian or Amazonian rainfall decadal variations (Fernandes et al., 2015; Knight et al., 2006; Martin et al., 2014; Zhang & Delworth, 2006). However, what has caused this rainfall link and the recent AMO phase change is not well understood, and a debate regarding the relative role of IV versus external forcing is still ongoing (Bellucci et al., 2017; Clement et al., 2015; Delworth & Mann, 2000; Murphy et al., 2017; Ting et al., 2009; Zhang et al., 2013, 2016). Here we investigate this issue through attribution analyses of the decadal rainfall seesaw pattern using ensemble climate model simulations.

3.2. Rainfall Variability in Coupled Model Simulations

The CanESM2-simulated rainfall decadal variations over the Sahel (SA) from most of its all-forcing ensemble simulations are positively correlated with the observations during 1950–2017, with a mean correlation of 0.57 (0.40; Figures 2a and 2b). This suggests that the CanESM2 model can reasonably reproduce the regional rainfall decadal variations (Figure S3), although the decadal variability of rainfall in Sahel and across the globe is weak in CMIP5 models (Ault et al., 2012). The rainfall data can be divided into two components: the forced signal as represented by the ensemble mean and IV as represented by the residual variations after removing the ensemble mean from individual simulations. The correlations between the modeled IV component from individual runs and observed regional rainfall anomalies for the Sahel (SA) have a mean around zero, with only 12% (13%) of them being statistically significant ($p = 0.05$), compared with 64% (32%) for the ALL simulations with the forced signal included (Figures 2a and 2b). This suggested that a significant fraction of Sahel's and SA's rainfall variations can be explained by the external forced component, and the correlations between the modeled and observed rainfall series are mainly due to the forced component. We therefore investigate additional simulations that are forced by different combinations of external factors (blue and green lines in Figure 2a and 2b). The results show that AA have contributed to the simulated Sahel (SA) rainfall decadal variations, with 46% (30%) of the simulations being statistically significant ($p = 0.05$), larger than the IV case. NAT also contributed to the Sahel (SA) rainfall variations, with 24% (30%) of the simulations being statistically significant ($p = 0.05$), also larger than the IV case (Figures 2a and 2b).

The Sahel and SA rainfall anomalies are also negatively correlated for most of the ensemble members in all the CanESM2 experiments and for the IV case (Figure 2c). However, significant anticorrelations ($p = 0.05$) between the Sahel and SA rainfall exist only in a smaller number (~7%, close to the 5% expected by random chances) of the simulations after removing the forced component (i.e., the IV case), compared with 26% for the ALL simulations with the forced signal included. Simulations forced by AA (NAT) forcing only show 16% (14%) of the simulations with significant
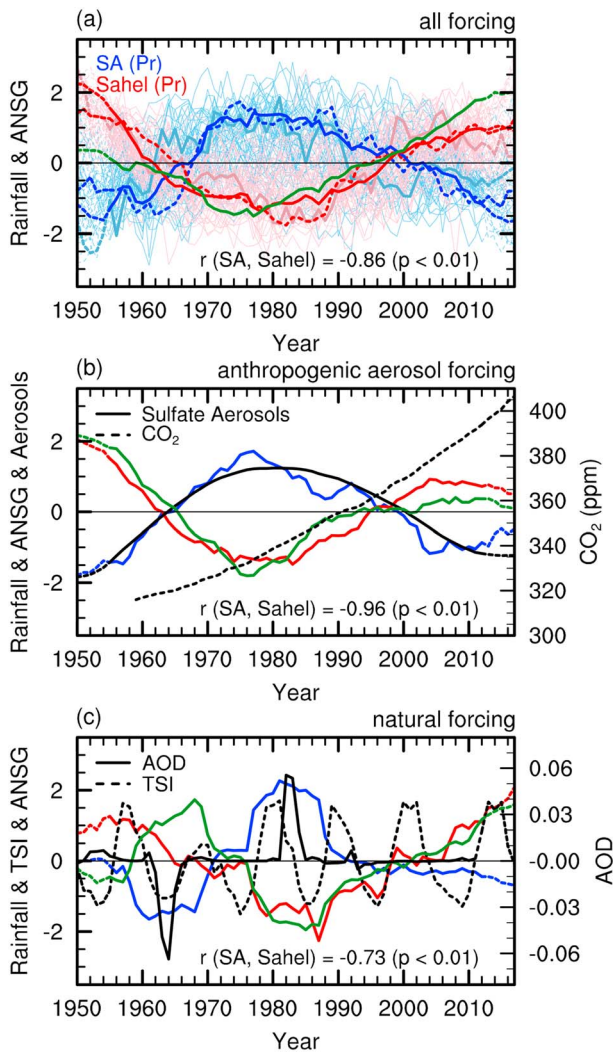
Figure 3. (a) Normalized time series of linearly detrended, 11-year smoothed July-August-September rainfall anomalies from observations (dotted lines), and Canadian Earth System Model version 2 historical all-forcing simulations (light solid lines) over the Sahel (red lines) and SA (blue lines). The thick solid lines indicate the ensemble mean, together with the normalized ANSG index (green line). The pink (bright blue) line is from one model run (#8) for the Sahel (SA). Also shown is the correlation coefficient (r) between the two regional rainfall anomalies from the ensemble mean. (b) Same as (a) but for the ensemble mean of the Canadian Earth System Model version 2 anthropogenic aerosol simulations. The black solid line represents the smoothed sulfate aerosol concentrations averaged over North America and Europe (0°N to 60°N, 120°W to 60°E), and the green solid line shows the normalized ANSG index from the anthropogenic aerosol simulations. The black dashed line indicates the observed atmospheric CO_2 concentrations (ppm, right ordinate). (c) Same as (a) but for the ensemble mean of the CanESM2 natural forcing simulations. The black solid line indicates the differences in the estimated stratospheric aerosol optical depth (AOD) between the Northern and Southern Hemispheric mean. The black dashed line represents the normalized annual mean of total solar irradiance (TSI). The ending points, plotted using dashed lines, used mirrored data in the running average and thus are less reliable. ANSG = Atlantic North-South SST gradient; SA = southeast Amazon.

anticorrelations between Sahel and SA rainfall (Figure 2c). Thus, while there exists a small (~7%) chance that IV can lead to significant anticorrelations between Sahel and SA rainfall during JAS, recent external forcing from both AA and NAT can substantially increase that chance (up to ~26%).

The physical processes underlying the rainfall seesaw pattern in the ensemble mean of CanESM2 simulations are similar to those in observations (Figures S5a and S5b). This suggests that the observed rainfall seesaw pattern and its underlying physical processes are mainly explained by the external forcing, rather than due to IV. Furthermore, the interhemispheric variations in Atlantic SSTs and ITCZ and the related atmospheric circulation changes also occur due to IV, leading to a significant rainfall anticorrelation in about 7% of the realizations for the IV case (Figures S5c and S5d), but the decadal variations caused by IV are typically not in phase with the observations (otherwise, they would show significant anticorrelations between the Sahel and SA rainfalls).

3.3. Causes of the Decadal Rainfall Seesaw Pattern

The decadal rainfall evolutions in most of the CanESM2 ALL ensemble simulations compare well with the observations (Figure 3a), but this is true only when the forced signal (i.e., the ensemble mean) is included in the simulated rainfall series. Sulfate aerosols from North America and Europe peaked in the 1970s and 1980s and covary with decadal rainfall variations since 1950, and the ensemble mean of the AA simulations captures well the rainfall seesaw pattern (Figure 3b). This suggests a major role of the AA in generating this pattern. The NAT simulations also show an inverse relationship between the Sahel and SA rainfall variations. This is mainly due to the recent volcanic eruptions by Agung in 1963 and El Chinchón in 1982 that caused decadal variations in the smoothed time series of the interhemispheric gradient in stratospheric aerosols and ANSG (Haywood et al., 2013; Otterå et al., 2010), and these decadal variations are correlated with the regional rainfall over both regions (Figure 3c). The solar irradiance changes are small and uncorrelated with the decadal rainfall variations (Figure 3c).

The above CanESM2 results are largely confirmed by the CMIP5 multi-model ensemble simulations (Figure S6). For example, the observed Sahel and SA rainfall decadal variations are reproduced mainly by the externally forced signals (e.g., AA and NAT), rather than by IV (Figure S6). However, current climate models still have substantial biases (Wang et al., 2014) and some of the CMIP5 models performed poorly in simulating the Sahel and SA rainfall and North Atlantic SSTs (Figure S3). These models generally underestimate the magnitude of observed IV for Sahel and SA rainfall, and different realizations of internal climate variability in different models also lead to a widespread among the models (e.g., Fyfe et al., 2013). Nevertheless, available model simulations (Figures S6 and S7) seem to suggest that the observed decadal rainfall variations in the Sahel and SA and their seesaw pattern since 1950 likely have resulted mainly from decadal changes in anthropogenic and volcanic aerosols, as the chance is small (~4% for the IV case, which is largely by random chances, compared with ~11% for the ALL, ~19% for the NAT, and ~23% for the AA case) for them to have resulted purely from IV.

Furthermore, the observed decadal SST variations in the North Atlantic are correlated significantly with those from most (>68%, $p < 0.05$) of the
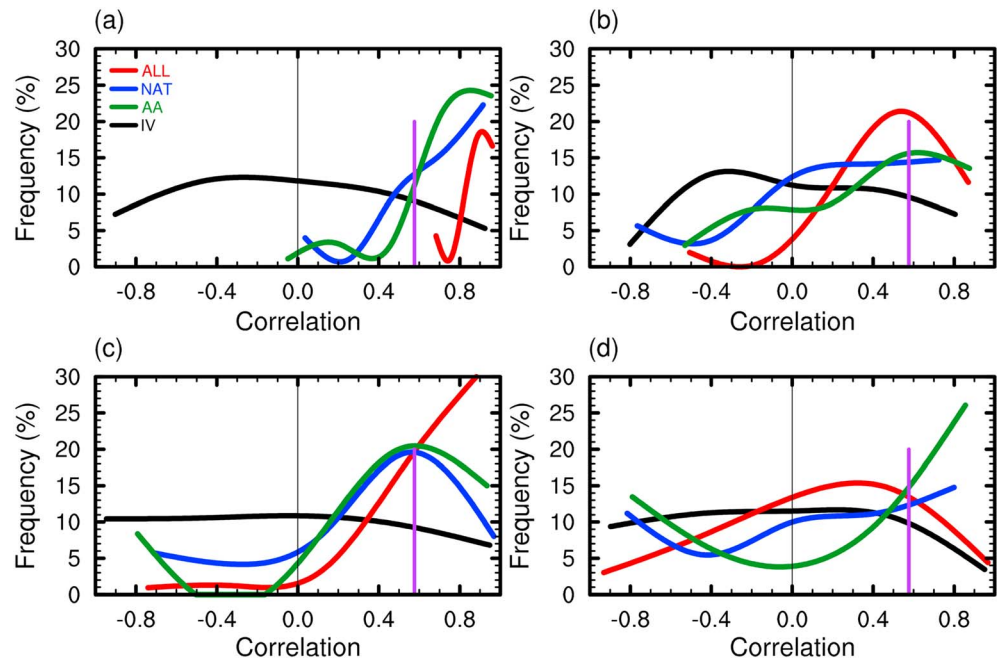
Figure 4. (a) Estimated histograms of the correlation coefficients during 1950–2017 between the observed and Canadian Earth System Model version 2 simulated North Atlantic mean sea surface temperature (SST) from individual model runs with all-forcing (ALL, red line), natural forcing only (NAT, blue line), and anthropogenic aerosol forcing only (AA, green line). The black line is for the internal variability (IV) case, in which the SST series from 150 individual members from the ALL, NAT, and AA simulations were first subtracted by their respective ensemble mean, smoothed using 11-year averaging, and then correlated with the 11-year smoothed SST time series from observations. The estimated histograms were fitted by a cubic spline to produce the curves shown here. (b) Same as (a) but for the Atlantic North-South gradient indices. (c) Same as (a) but for the phase 5 of the Coupled Model Intercomparison Project multimodel ensemble simulations during the period 1950–2005. (d) Same as (b) but for the phase 5 of the Coupled Model Intercomparison Project multimodel ensemble simulations during the period 1950–2005. The purple vertical line indicates the significant r value at the 0.05 level for all cases.

CanESM2 and CMIP5 simulations forced with all-forcing (Figure 4). The number of the simulations correlated with the observations in the AA and NAT only simulations decreases to ~42% and 45%, respectively, but it is still much larger than that (~16%) in the IV case. Similar results are found for ANSG (Figure 4). These model results are consistent with many previous studies (Booth et al., 2012; Murphy et al., 2017; Otterå et al., 2010) that suggest a major role of external forcing in generating the recent North Atlantic decadal to multidecadal variations and support the notion that the observed North Atlantic SSTs since 1950 likely have resulted mainly from decadal changes in anthropogenic (mainly from North America and Europe) and volcanic aerosols, rather than IV.

4. Conclusions and Discussion

In this study, we have shown an anticorrelated seesaw pattern in JAS rainfall over the Sahel and SA during 1950–2017 in both observations and coupled model simulations. An anomalous meridional SST gradient across the tropical Atlantic pushes the ITCZ and its associated rain belt toward the anomalously warm hemisphere (e.g., the Southern Hemisphere during the 1970s and 1980s and the Northern Hemisphere during the 1950s and 2000s). Large ensemble simulations by the CanESM2 and other CMIP5 models suggest that these decadal variations in the tropical SST gradient, the ITCZ, and the associated rainfall seesaw pattern over the Sahel and SA likely have resulted primarily from decadal changes in anthropogenic and volcanic aerosols, rather than internal climate variability.

Our findings are consistent with previous notion that NAT has caused the tropical rain belt to shift on decadal time scales, and AA forcing may help maintain and intensify tropical rainfall variations and contribute to the most recent North Atlantic decadal to multidecadal variations (e.g., Allen et al., 2015; Hwang

et al., 2013). Here we have further shown that changes in both the anthropogenic and volcanic aerosols likely have contributed to the recent AMO and to the rainfall decadal variations over the Sahel and SA and their anticorrelation since 1950, while the chance for these decadal variations to have resulted purely from IV is small (<16%, compared with 68% in the ALL case). Thus, our results support the notion of a forced North Atlantic decadal to multidecadal variability during the latter half of the twentieth century.

Our results highlight the importance of the external forcing from anthropogenic and volcanic aerosols for recent decadal climate variations in and around the North Atlantic Ocean. However, current simulations of the aerosol forcing, especially aerosols' indirect effects, still have large uncertainties (Hua et al., 2018; Sato et al., 2018; Zhang et al., 2013). Bellucci et al. (2017) demonstrated that it is necessary to include the aerosol indirect effects in CMIP5 models in order to capture the observed Atlantic SST variations. Further efforts to reduce the model deficiencies in simulating aerosol-cloud interactions, especially aerosols' indirect effects on cloud albedo and lifetime, could help improve simulations of the externally forced climate variations and advance our understanding of decadal variability in the Atlantic (Boucher et al., 2013).

Looking ahead into the future, GHGs will continue to increase, whereas sulfate aerosols over North America and Europe have decreased since the late 1970s and will continue to decrease in the future (Collins et al., 2013). Model projections for the 21st century point to larger warming in the North Atlantic than in the South Atlantic (Hoerling et al., 2006), which will likely cause a northward shift of the ITCZ and thus a wetting (drying) trend over the Sahel (SA) on top of warming-induced other changes based on our findings (Figure S8). This opposite change pattern over these two hot spot regions is consistent with model projections of increased (decreased) rainfall in the Sahel (Amazon) in the 21st century (Zhao & Dai, 2017).

References

Allen, R. J., Evan, A. T., & Booth, B. B. B. (2015). Interhemispheric aerosol radiative forcing and tropical precipitation shifts during the late twentieth century. *Journal of Climate*, 28(20), 8219–8246. https://doi.org/10.1175/JCLI-D-15-0148.1

Ault, T. R., Cole, J. E., & George, S. S. (2012). The amplitude of decadal to multidecadal variability in precipitation simulated by state-of-the-art climate models. *Geophysical Research Letters*, 39, L21705. https://doi.org/10.1029/2012GL053424

Baines, P. G., & Folland, C. K. (2007). Evidence for a rapid global climate shift across the late 1960s. *Journal of Climate*, 20(12), 2721–2744. https://doi.org/10.1175/JCLI4177.1

Bellucci, A., Mariotti, A., & Gualdi, S. (2017). The role of forcings in the twentieth-century North Atlantic multidecadal variability: The 1940–75 North Atlantic cooling case study. *Journal of Climate*, 30(18), 7317–7337. https://doi.org/10.1175/JCLI-D-16-0301.1

Biasutti, M., & Giannini, A. (2006). Robust Sahel drying in response to late 20th century forcings. *Geophysical Research Letters*, 33, L11706. https://doi.org/10.1029/2006GL026067

Booth, B. B. B., Dunstone, N. J., Halloran, P. R., Andrews, T., & Bellouin, N. (2012). Aerosols implicated as a prime driver of twentieth-century North Atlantic climate variability. *Nature*, 484(7393), 228–232. https://doi.org/10.1038/nature10946

Boucher, O., Randall, D., Artaxo, P., Bretherton, C., Feingold, G., Forster, P., et al. (2013). Clouds and aerosols. In climate change 2013: The physical science basis. In *Contribution of working group I to the fifth assessment report of the intergovernmental panel on climate change* (pp. 571–658). Cambridge, UK and New York: Cambridge University press.

Chen, M., Xie, P., Janowiak, J. E., & Arkin, P. A. (2002). Global land precipitation: A 50-yr monthly analysis based on gauge observations. *Journal of Hydrometeorology*, 3, 249–266. https://doi.org/10.1175/1525-7541(2002)003<0249:GLPAYM>2.0.CO;2

Clement, A., Bellomo, K., Murphy, L. N., Cane, M. A., Mauritsen, T., Rädel, G., & Stevens, B. (2015). The Atlantic Multidecadal Oscillation without a role for ocean circulation. *Science*, 350(6258), 320–324. https://doi.org/10.1126/science.aab3980

Collins, M., Knutti, R., Arblaster, J., Dufresne, J.-L., Fichefet, T., Friedlingstein, P., et al. (2013). Long-term climate change: Projections, commitments and irreversibility. In *Climate change 2013: The physical science basis. Contribution of working group I to the fifth assessment report of the intergovernmental panel on climate change* (pp. 1029–1136). Cambridge, UK and New York: Cambridge University Press. https://doi.org/10.1017/CBO9781107415324.024

Cox, P. M., Harris, P. P., Huntingford, C., Betts, R. A., Collins, M., & Jones, C. D. (2008). Increasing risk of Amazonian drought due to decreasing aerosol pollution. *Nature*, 453(7192), 212–215. https://doi.org/10.1038/nature06960

Dai, A., & Bloecker, C. E. (2018). Impacts of internal variability on temperature and precipitation trends in large ensemble simulations by two climate models. *Climate Dynamics*. https://doi.org/10.1007/s00382-018-4132-4

Dai, A., Fyfe, J. C., Xie, S.-P., & Dai, X. (2015). Decadal modulation of global surface temperature by internal climate variability. *Nature Climate Change*, 5(6), 555–559. https://doi.org/10.1038/nclimate2605

Dai, A., Lamb, P. J., Trenberth, K. E., Hulme, M., Jones, P. D., & Xie, P. (2004). The recent Sahel drought is real. *International Journal of Climatology*, 24(11), 1323–1331. https://doi.org/10.1002/joc.1083

Delworth, T. L., & Mann, M. E. (2000). Observed and simulated multidecadal variability in the Northern Hemisphere. *Climate Dynamics*, 16(9), 661–676. https://doi.org/10.1007/s003820000075

Dong, B., & Sutton, R. (2015). Dominant role of greenhouse-gas forcing in the recovery of Sahel rainfall. *Nature Climate Change*, 5(8), 757–760. https://doi.org/10.1038/nclimate2664

Fernandes, K., Giannini, A., Verchot, L., Baethgen, W., & Pinedo-Vasquez, M. (2015). Decadal covariability of Atlantic SSTs and western Amazon dry-season hydroclimate in observations and CMIP5 simulations. *Geophysical Research Letters*, 42, 6793–6801. https://doi.org/10.1002/2015GL063911

Folland, C. K., Palmer, T. N., & Parker, D. E. (1986). Sahel rainfall and worldwide sea temperatures, 1901–85. *Nature*, 320(6063), 602–607. https://doi.org/10.1038/320602a0

Frankcombe, L. M., England, M. H., Kajtar, J. B., Mann, M. E., & Steinman, B. A. (2018). On the choice of ensemble mean for estimating the forced signal in the presence of internal variability. *Journal of Climate*, *31*(14), 5681–5693. https://doi.org/10.1175/JCLI-D-17-0662.1

Frankcombe, L. M., England, M. H., Mann, M. E., & Steinman, B. A. (2015). Separating internal variability from the externally forced climate response. *Journal of Climate*, *28*(20), 8184–8202. https://doi.org/10.1175/JCLI-D-15-0069.1

Fyfe, J. C., Gillett, N. P., & Zwiers, F. W. (2013). Overestimated global warming over the past 20 years. *Nature Climate Change*, *3*(9), 767–769. https://doi.org/10.1038/nclimate1972

Giannini, A., Saravanan, R., & Chang, P. (2003). Oceanic forcing of Sahel rainfall on interannual to interdecadal time scales. *Science*, *302*(5647), 1027–1030. https://doi.org/10.1126/science.1089357

Hagos, S. M., & Cook, K. H. (2008). Ocean warming and late-twentieth-century Sahel drought and recovery. *Journal of Climate*, *21*(15), 3797–3814. https://doi.org/10.1175/2008JCLI2055.1

Harris, I., Jones, P. D., Osborn, T. J., & Lister, D. H. (2014). Updated high-resolution grids of monthly climatic observations—The CRU TS3.10 Dataset. *International Journal of Climatology*, *34*(3), 623–642. https://doi.org/10.1002/joc.3711

Haywood, J. M., Jones, A., Bellouin, N., & Stephenson, D. (2013). Asymmetric forcing from stratospheric aerosols impacts Sahelian rainfall. *Nature Climate Change*, *3*(7), 660–665. https://doi.org/10.1038/nclimate1857

Held, I. M., Delworth, T. L., Lu, J., Findell, K. L., & Knutson, T. R. (2005). Simulation of Sahel drought in the 20th and 21st centuries. *Proceedings of the National Academy of Sciences of the United States of America*, *102*(50), 17,891–17,896. https://doi.org/10.1073/pnas.0509057102

Hoerling, M., Hurrell, J., Eischeid, J., & Phillips, A. (2006). Detection and attribution of twentieth-century northern and southern African rainfall change. *Journal of Climate*, *19*(16), 3989–4008. https://doi.org/10.1175/JCLI3842.1

Hua, W., Dai, A., & Qin, M. (2018). Contributions of internal variability and external forcing to the recent pacific decadal variations. *Geophysical Research Letters*, *45*, 7084–7092. https://doi.org/10.1029/2018GL079033

Hurrell, J. W., Hack, J. J., Shea, D., Caron, J. M., & Rosinski, J. (2008). A new sea surface temperature and sea ice boundary dataset for the Community Atmosphere Model. *Journal of Climate*, *21*(19), 5145–5153. https://doi.org/10.1175/2008JCLI2292.1

Hwang, Y.-T., Frierson, D. M. W., & Kang, S. M. (2013). Anthropogenic sulfate aerosol and the southward shift of tropical precipitation in the late 20th century. *Geophysical Research Letters*, *40*, 2845–2850. https://doi.org/10.1002/grl.50502

Jones, P. D., & Moberg, A. (2003). Hemispheric and large-scale surface air temperature variations: An extensive revision and an update to 2001. *Journal of Climate*, *16*(2), 206–223. https://doi.org/10.1175/1520-0442(2003)016<0206:HALSSA>2.0.CO;2

Kalnay, E., Kanamitsu, M., Kistler, R., Collins, W., Deaven, D., Gandin, L., et al. (1996). The NCEP/NCAR 40-year reanalysis project. *Bulletin of the American Meteorological Society*, *77*(3), 437–471. https://doi.org/10.1175/1520-0477(1996)077<0437:TNYRP>2.0.CO;2

Kirchmeier-Young, M. C., Zwiers, F. W., & Gillett, N. P. (2017). Attribution of extreme events in Arctic Sea ice extent. *Journal of Climate*, *30*(2), 553–571. https://doi.org/10.1175/JCLI-D-16-0412.1

Knight, J. R., Folland, C. K., & Scaife, A. A. (2006). Climate impacts of the Atlantic Multidecadal Oscillation. *Geophysical Research Letters*, *33*, L17706. https://doi.org/10.1029/2006GL026242

Lamb, P. J., & Peppler, R. A. (1992). Further case studies of tropical Atlantic surface atmospheric and oceanic patterns associated with sub-Saharan drought. *Journal of Climate*, *5*(5), 476–488. https://doi.org/10.1175/1520-0442(1992)005<0476:FCSOTA>2.0.CO;2

Lean, J. (2000). Evolution of the Sun's spectral irradiance since the maunder minimum. *Geophysical Research Letters*, *27*, 2425–2428. https://doi.org/10.1029/2000GL000043

Lewis, S. L., Brando, P. M., Phillips, O. L., van der Heijden, G. M. F., & Nepstad, D. (2011). The 2010 Amazon drought. *Science*, *331*(6017), 554. https://doi.org/10.1126/science.1200807

Malhi, Y., Roberts, J. T., Betts, R. A., Killeen, T. J., Li, W., & Nobre, C. A. (2008). Climate change, deforestation, and the fate of the Amazon. *Science*, *319*(5860), 169–172. https://doi.org/10.1126/science.1146961

Marengo, J. A., Tomasella, J., Alves, L. M., Soares, W. R., & Rodriguez, D. A. (2011). The drought of 2010 in the context of historical droughts in the Amazon region. *Geophysical Research Letters*, *38*, L12703. https://doi.org/10.1029/2011GL047436

Martin, E. R., Thorncroft, C., & Booth, B. B. (2014). The multidecadal Atlantic SST–Sahel rainfall teleconnection in CMIP5 simulations. *Journal of Climate*, *27*(2), 784–806. https://doi.org/10.1175/JCLI-D-13-00242.1

Monerie, P. A., Sanchez-Gomez, E., Pohl, B., Robson, J., & Dong, B. (2017). Impact of internal variability on projections of Sahel precipitation change. *Environmental Research Letters*, *12*, 114003. https://doi.org/10.1088/1748-9326/aa8cda

Murphy, L. N., Bellomo, K., Cane, M., & Clement, A. (2017). The role of historical forcings in simulating the observed Atlantic multidecadal oscillation. *Geophysical Research Letters*, *44*, 2472–2480. https://doi.org/10.1002/2016GL071337

Otterå, O. H., Bentsen, M., Drange, H., & Suo, L. (2010). External forcing as a metronome for Atlantic multidecadal variability. *Nature Geoscience*, *3*(10), 688–694. https://doi.org/10.1038/ngeo955

Palmer, T. N. (1986). Influence of the Atlantic, Pacific and Indian Oceans on Sahel rainfall. *Nature*, *322*(6076), 251–253. https://doi.org/10.1038/322251a0

Park, J.-Y., Bader, J., & Matei, D. (2016). Anthropogenic Mediterranean warming essential driver for present and future Sahel rainfall. *Nature Climate Change*, *6*(10), 941–945. https://doi.org/10.1038/nclimate3065

Peterson, T. C., & Vose, R. S. (1997). An overview of the global historical climatology network temperature data base. *Bulletin of the American Meteorological Society*, *78*(12), 2837–2849. https://doi.org/10.1175/1520-0477(1997)078<2837:AOOTGH>2.0.CO;2

Rowell, D. P. (2003). The impact of Mediterranean SSTs on the Sahelian rainfall season. *Journal of Climate*, *16*(5), 849–862. https://doi.org/10.1175/1520-0442(2003)016<0849:TIOMSO>2.0.CO;2

Sato, M., Hansen, J. E., McCormick, M. P., & Pollack, J. B. (1993). Stratospheric aerosol optical depth, 1850-1990. *Journal of Geophysical Research*, *98*, 22,987–22,994. https://doi.org/10.1029/93JD02553

Sato, Y., Goto, D., Michibata, T., Suzuki, K., Takemura, T., Tomita, H., & Nakajima, T. (2018). Aerosol effects on cloud water amounts were successfully simulated by a global cloud-system resolving model. *Nature Communications*, *9*(1), 985. https://doi.org/10.1038/s41467-018-03379-6

Schneider, U., Becker, A., Finger, P., Meyer-Christoffer, A., Ziese, M., & Rudolf, B. (2014). GPCC's new land surface precipitation climatology based on quality-controlled in situ data and its role in quantifying the global water cycle. *Theoretical and Applied Climatology*, *115*(1-2), 15–40. https://doi.org/10.1007/s00704-013-0860-x

Shanahan, T. M., Overpeck, J. T., Anchukaitis, K. J., Beck, J. W., Cole, J. E., Dettman, D. L., et al. (2009). Atlantic forcing of persistent drought in West Africa. *Science*, *324*(5925), 377–380. https://doi.org/10.1126/science.1166352

Sheen, K. L., Smith, D. M., Dunstone, N. J., Eade, R., Rowell, D. P., & Vellinga, M. (2017). Skillful prediction of Sahel summer rainfall on inter-annual and multi-year timescales. *Nature Communications*, *8*, 14966. https://doi.org/10.1038/ncomms14966

Steinman, B. A., Mann, M. E., & Miller, S. K. (2015). Atlantic and Pacific multidecadal oscillations and Northern Hemisphere temperatures. *Science*, *347*(6225), 988–991. https://doi.org/10.1126/science.1257856

Taylor, K. E., Stouffer, R. J., & Meehl, G. A. (2012). An overview of CMIP5 and the experiment design. *Bulletin of the American Meteorological Society*, *93*(4), 485–498. https://doi.org/10.1175/BAMS-D-11-00094.1

Ting, M., Kushnir, Y., Seager, R., & Li, C. (2009). Forced and internal twentieth-century SST in the North Atlantic. *Journal of Climate*, *22*(6), 1469–1481. https://doi.org/10.1175/2008JCLI2561.1

Trenberth, K. E., & Shea, D. J. (2006). Atlantic hurricanes and natural variability in 2005. *Geophysical Research Letters*, *33*, L12704. https://doi.org/10.1029/2006GL026894

Vecchi, G. A., Delworth, T. L., & Booth, B. (2017). Climate science: Origins of Atlantic decadal swings. *Nature*, *548*(7667), 284–285. https://doi.org/10.1038/nature23538

Wang, C., Zhang, L., Lee, S. K., Wu, L., & Mechoso, C. R. (2014). A global perspective on CMIP5 climate model biases. *Nature Climate Change*, *4*(3), 201–205. https://doi.org/10.1038/nclimate2118

Wang, Y.-M., Lean, J. L., & Sheeley, N. R. Jr. (2005). Modeling the Sun's magnetic field and irradiance since 1713. *The Astrophysical Journal*, *625*(1), 522–538. https://doi.org/10.1086/429689

Willmott, C. J., & Matsuura, K. (2001). Terrestrial air temperature and precipitation: Monthly and annual time series (1950–1999). Retrieved from http://climate.geog.udel.edu/~climate/html_pages/README.ghcn_ts2.html

Yoon, J. H., & Zeng, N. (2010). An Atlantic influence on Amazon rainfall. *Climate Dynamics*, *34*(2-3), 249–264. https://doi.org/10.1007/s00382-009-0551-6

Zeng, N., Yoon, J. H., Marengo, J. A., Subramaniam, A., Nobre, C. A., Mariotti, A., & Neelin, J. D. (2008). Causes and impacts of the 2005 Amazon drought. *Environmental Research Letters*, *3*(1), 014002. https://doi.org/10.1088/1748-9326/3/1/014002

Zhang, R., & Delworth, T. L. (2006). Impact of Atlantic multidecadal oscillations on India/Sahel rainfall and Atlantic hurricanes. *Geophysical Research Letters*, *33*, L17712. https://doi.org/10.1029/2006GL026267

Zhang, R., Delworth, T. L., Sutton, R., Hodson, D. L. R., Dixon, K. W., Held, I. M., et al. (2013). Have aerosols caused the observed Atlantic multidecadal variability? *Journal of the Atmospheric Sciences*, *70*(4), 1135–1144. https://doi.org/10.1175/JAS-D-12-0331.1

Zhang, R., Sutton, R., Danabasoglu, G., Delworth, T. L., Kim, W. M., Robson, J., & Yeager, S. G. (2016). Comment on "The Atlantic Multidecadal Oscillation without a role for ocean circulation". *Science*, *352*(6293), 1527–1527. https://doi.org/10.1126/science.aaf1660

Zhao, T., & Dai, A. (2017). Uncertainties in historical changes and future projections of drought. Part II: Model-simulated historical and future drought changes. *Climatic Change*, *144*(3), 535–548. https://doi.org/10.1007/s10584-016-1742-x

Zhao, W., & Khalil, M. A. K. (1993). The relationship between precipitation and temperature over the contiguous United States. *Journal of Climate*, *6*(6), 1232–1236. https://doi.org/10.1175/1520-0442(1993)006<1232:TRBPAT>2.0.CO;2